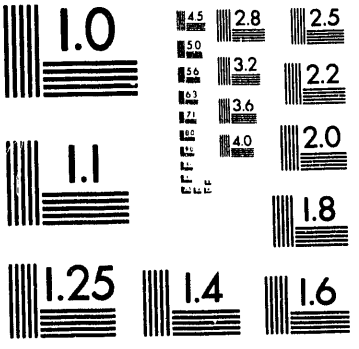
1.0
1.1
1.25
1.4
1.6
1.8
2.0
2.2
2.5
2.8
3.2
3.6
4.0
4.5
5.0
5.6
6.3
7.1
8.0
9.0

1 of 1

Time-of-Flight Heavy Ion Backscattering Spectrometry

J.A. Knapp, J.C. Banks, and B.L. Doyle

Sandia National Laboratories

Albuquerque, New Mexico 87185, USA

Abstract

A new time-of-flight (TOF) ion detection system for Heavy Ion Backscattering Spectrometry (HIBS) is described. Examples are also given of the use of the system for measuring low-level contamination on Si wafers. Currently, the TOF-HIBS system has a sensitivity of $1x10^9/cm^2$ for the heaviest of surface impurity atoms and a mass resolution capable of separating Fe from Cu. The sensitivity is expected to improve by an additional order of magnitude on a industrial TOF-HIBS system being constructed for SEMATECH.

1. Introduction

For many new problems in materials research, particularly for contamination control in microelectronics, the sensitivity to surface impurities in conventional Rutherford Backscattering Spectrometry (RBS) is only marginally adequate. For example, by the turn of the century, very large scale integrated circuit processing will require contamination levels well below $1x10^9$ atoms/cm^2 in both starting materials and introduced by processing.[1] The most sensitive of existing general-purpose tools, total reflection x-ray fluorescence (TXRF), can detect ~$1x10^{10}$ atoms/cm^2 levels of some elements such as Fe and Cu, but for many others it is limited to $1x10^{12}$ atoms/cm^2 or

worse. Furthermore, there are significant ranges of the periodic table where TXRF is completely insensitive.

As an alternative to existing tools and as a means for an absolute calibration of other methods such as TXRF, we have been developing a new approach[2-4] to backscattering analysis using moderate energy (a few hundred keV) heavy ions, called Heavy Ion Backscattering Spectrometry (HIBS). HIBS has already demonstrated sensitivity for medium-to-heavy impurities on Si more than 1000x greater than RBS. The basis for the increased sensitivity is the well-known proportionality of backscattering yield to the atomic number of the beam, divided by its energy, both squared ($Y \propto Z^2/E^2$). Unfortunately, because yield from the substrate is increased as much as the signal from the impurities of interest, pulse pileup is a severe problem. The key innovation in HIBS is the reduction of this pileup by placing a thin foil in front of the detector. This foil ranges out ions scattered from the substrate but allows ions scattered from near-surface impurities heavier than the substrate to reach the detector.

Our early implementations of HIBS [2-4] used a standard Si surface barrier particle detector (SBD), which has the advantages of simplicity and compact size. A system with three parallel SBD detectors, each with its own thin C foil, gave sensitivities of ~$5x10^{10}$ atoms/cm^2 for Fe on Si and ~$5x10^8$ atoms/cm^2 for Au, using 200-400 keV C^+ and N^+ beams. However, an SBD is not well suited to this application, both because of the limits to its energy resolution and the presence of a dead layer at the surface. The energy resolution severely limits the mass resolution which can be achieved, making it difficult to separate contributions from Fe and Cu, for example. The dead layer adds an additional effective thickness to the foil, which increases straggling and limits the usable beam energy for say carbon ions to 200 keV or above for impurities on Si. Still, for some dedicated applications where these limitations would not matter, HIBS using a SBD is a cost-effective and extremely simple solution.

2. Time-of-Flight HIBS

Despite the fact that a time-of-flight (TOF) ion detection scheme is more complicated and expensive to set up, the much better energy resolution which can be obtained makes such a detector worthwhile. The improved resolution allows better separation of masses, particularly in the low mass range, and that together with greater efficiency at low detected ion energy allows the system to be operated with analysis beams as low as 100 keV. The use of such low-energy ions in turn gives more sensitivity as the cross-section increases, and is limited only by straggling in the foil and the lower efficiency of the ion detector used for detecting the scattered particles, also at lower energies.

We reported earlier[4] on a prototype TOF-HIBS detector, designed to take advantage of our existing analysis chamber while testing the concept of a large solid angle TOF detector. The results were promising enough that an entirely new, larger chamber was fabricated and a new system assembled, with improvements designed to fix the technological problems encountered in the prototype. Figure 1 is a schematic of the new TOF-HIBS detector. The TOF detector system consists of two event timing detectors. As backscattered ions pass through the thin C foil, they produce secondary electrons which are accelerated through an adjacent grid and detected by the electron microchannel plate assembly, called the electron MCP in the figure, and produce a timing pulse. The ions continue their flight until stopped in the ion MCP, giving another timing pulse.

The ion beam is defined to 2 mm diameter with an aperture and then enters the chamber through a flight tube (not shown), leaving the tube a few cm before striking the sample. Both the aperture and flight tube are made from high purity aluminum. The samples are mounted on a 6 position, 2-axis goniometer, with only high purity Al or low Z material used for mounting. Backscattered particles pass through a 5 $\mu g/cm^2$ C foil, mounted on a 90% transmitting Ni grid and biased at -400V relative to ground. A second grid, at ground potential, is mounted 2.5 mm away at the back side of the foil. The foil

serves two purposes: one, to range out the particles scattered from the light substrate, as in the SBD approach to HIBS, and second, to provide a pulse of electrons, which is detected by the electron MCP assembly (Galileo Electro-Optics FTD-2003). Particles which exit the foil (in principle only those scattered from heavy impurities) pass along a 14.7 cm flight path and are detected by the ion MCP assembly (Galileo Electro-Optics FTD-4000). Both assemblies use chevron MCP arrangements (two microchannel plates mounted and oriented to reduce feedback and increase gain). The front plate of the ion MCP assembly has a 1260 mm^2 active area.

Since it was desirable to maximize the solid angle for improving sensitivity, the angle subtended by the ion MCP is relatively large, which leads to kinematic broadening. That is, the kinematic factor for each mass changes substantially from one side of the plate to the other. The angles of both the foil and the ion MCP were chosen by computer simulation of our expected typical operating parameters to minimize this broadening. The foil and associated electron MCP are at 55° relative to the sample plane, while the ion MCP is at 20°. The backscattering angle at the center of the ion MCP is 164°, so this plate is tilted 4° away from being perpendicular to the average backscattered path.

This detector differs from our first prototype[4] in several important ways. First, the microchannel plate assemblies now have impedance matching conical anodes mounted on 50Ω BNC output connectors, for greatly improved resistance to system noise and ringing. Unfortunately, for the electron MCP the use of a BNC connector makes it more difficult to pass the signal through the chamber wall, since the front plate needs to be at ground, with the back plate, or signal at +2000 V. Standard 50Ω feedthroughs do not handle such high voltages. We took advantage of a decoupling system (Xenotech FTD-2003 Fast Pulse Decoupler) designed to solve this problem by Mendenhall and Weller in the course of their own research into the use of TOF detectors for low energy ion beam analysis.[5] The last major difference is that the ion MCP is mounted on a linear feedthrough such that it can be retracted 15 cm, and thereby doubling the flight path.

This allows trading off sensitivity (solid angle) for somewhat improved mass resolution in specific experiments. The solid angle for the MCP in the short flight path is 34 msr, while for the long flight path it is 11 msr.

After the signals are detected by the MCPs, the signals are amplified with fast preamps (Phillips Scientific 9654B-20) and passed through a constant fraction discriminator (Ortec 935). The electron MCP signal is then delayed by 300-500 ns, and the ion MCP pulse is used as the start pulse in a time-to-amplitude converter (Ortec 567), with the delayed electron pulse serving for the stop pulse. This configuration increases the efficiency of the detector (since only counts that are significant start the timing sequence).

3. Examples

Several examples will now be given illustrating the utility and resolution of the system. The first example, shown in Fig. 2, is of two pieces of Si wafer which have been deliberately contaminated with both Fe and Cu by ashing a spun-on, dosed photoresist. When these samples were examined with our earlier SBD-HIBS system, the contributions to the spectra from Fe and Cu could not be separated. Figure 2(a) clearly shows two peaks from the Fe and Cu, as well as a peak from Sb or Sn. Further improvements to the mass resolution should be achievable with optimization of the ranging foil thickness and uniformity. Part (b) of Fig. 2 is from a similar wafer, dosed as before and then cleaned using an HF vapor technique. The spectrum clearly shows that this particular cleaning sequence is more efficient for Fe than for Cu.

The second example, shown in Fig. 3, is from two samples of Si implanted with low doses of Pb at 20 keV. The first, shown in (a), was implanted with a nominal $1x10^{11}$ Pb/cm^2, while the second, shown in (b), was implanted with a nominal $1x10^{10}$ Pb/cm^2. The Cu contamination evident on both pieces was present on the starting wafer and

additional Cu was sputtered onto the Si sample from the beam defining slits used in the implanter. This accounts for the increased amount of Cu seen with the larger Pb implant dose. TRIM [6] calculations of the 20 keV implants predict an implant profile peaked at 17.5 nm. The surface position for Pb is marked on the figure, as well as the peak of the Pb distribution. This example clearly shows the capability of HIBS for high depth resolution profiling of shallow implants at low levels.

The final example is taken from a study comparing different trace analysis techniques.[7] In this case, a series of samples were dosed with different levels of Ni. The nominal doses associated with each spectrum: (a) $1x10^{13}$ Ni/cm^2, (b) $2x10^{12}$ Ni/cm^2, and (c) $5x10^{11}$ Ni/cm^2. HIBS confirms these levels of Ni and also demonstrates that the samples were contaminated with Br and low levels of Sb or Sn. Although the same samples were examined with TXRF at another laboratory, these contaminants were missed. This illustrates that even though the elemental identification capability of HIBS is perhaps not quite as good as other techniques (e.g. TXRF), the lack of matrix effects and general sensitivity to all elements above Ar is very powerful.

4. Limits to Sensitivity

Some of the limits to improving sensitivity in HIBS are: pulse pileup, multiple scattering, straggling in the foil, detector efficiency, and sputtering. Pulse pileup is largely eliminated by the range-timing foil, but because of energy straggling, non-uniformities in this foil, and the Matsunami effect [8] some particles scattered from the substrate come through the foil, producing a background at lower flight time (see Figs. 2-4) and a small amount of pileup. Multiple scattering, where particles undergo several small angle scattering events and exit the sample with higher energy than a single large-angle event would produce, is expected to produce a background at very low levels.[9] Straggling in the foil is a more serious effect, dominating the observed time resolution and limiting the mass resolution that can be achieved. The efficiency of the microchannel

plates, especially for low energy ions, is an unknown, but our observations suggest that they are less effective at low energy. This reduces the overall efficiency and sensitivity of the detector as the beam energy is reduced, eventually negating the gain in yield at lower energy. Sputtering is the ultimate limit to the statistics which can be obtained, and hence the sensitivity. The rate of sputtering will depend on the state of the impurity: particles will sputter differently than widely dispersed, low concentration layers, so it is difficult to predict the limit in advance. Preliminary experiments suggest that the rate for a sub-monolayer impurity is lower than predicted by a simple sputtering model using bulk sputtering rates.

The sensitivity of the system in its present configuration ranges from ~$4x10^{10}$ atoms/cm^2 for Fe to ~$1x10^9$ atoms/cm^2 for Au. Further work with this system will concentrate on optimizing the thickness and uniformity of the foil. We will also increase the solid angle by installing a second, parallel TOF detector identical to the first. With three parallel detectors, optimized foils and a larger beam spot, we anticipate that ultimate sensitivities of $5x10^9$ for Fe and $1x10^8$ atoms/cm^2 for Au can be achieved. The overall accuracy of our current TOF-HIBS system has been estimated to be $((.05)^2+S^2))^{1/2}$, where S is the usual relative statistical error of the measurement.

Acknowledgments

The collaboration of P.J. Resnick and A.C. Diebold in studies of contamination of Si was essential. Technical assistance by D.L. Buller and K.G. Minor is gratefully acknowledged. This work was performed at Sandia National Laboratories and supported by the U.S. Department of Energy under contract no. DE-AC04-76DP00789.

References

[1] A.C. Diebold, P. Maillot, M. Gordon, J. Baylis, J. Chacon, R. Witowski, H.F. Arlinghaus, J.A. Knapp and B.L. Doyle, J. Vac. Sci. Technol. A10(4) (1992) 2945.

[2] B.L. Doyle, J.A. Knapp and D.L. Buller, Nucl. Instr. and Meth. B42 (1989) 295.

[3] J.A. Knapp and B.L. Doyle, Nucl. Instr. and Meth. B45 (1990) 143.

[4] J.A. Knapp and J.C. Banks, Nucl. Instr. and Meth. (in press).

[5] M.H. Mendenhall and R.A. Weller, Nucl. Instr. and Meth. B47 (1990) 193.

[6] TRIM-90 computer code, J.F. Ziegler, IBM Research Center, Yorktown Heights, New York, see also, J.F. Ziegler, J.P. Biersack, and U. Littmark, The Stopping and Range of Ions in Solids, Vol. 1 (Pergamon Press, New York, 1985)

[7] W.F. Calaway, S.R. Coon, M.J. Pellin, D.M. Gruen, M. Gordon, A.C. Diebold, P. Maillot, J.C. Banks, and J.A. Knapp, Surface and Interface Analysis (in press).

[8] N. Matsunami and K. Kitoh, Nucl. Instr. and Meth. B67 (1992) 50.

[9] D.K Brice, Nucl. Instr. and Meth. B69 (1992) 349.

Figure Captions

Fig. 1. Diagram of the Time-of-Flight HIBS detector system, in the short flight path configuration. The ion MCP is mounted on a linear feedthrough, so that the flight path can be doubled, increasing mass resolution at the expense of solid angle and sensitivity.

Fig. 2. Two TOF-HIBS spectra obtained with 150 keV N^+. Normalized yield is plotted versus flight time (decreasing from left to right so that detected energy (which is non-linear) increases from left to right). (A) Si doped with Fe and Cu by spin-on resist deposition and ashing. (B) A similar wafer after cleaning via an HF vapor technique. The Fe is greatly reduced by this cleaning procedure, but the Cu is not.

Fig. 3. Two TOF-HIBS spectra obtained with 150 keV N^+. Normalized yield is plotted versus flight time (decreasing from left to right). (A) Si implanted with a nominal $1x10^{11}$ Pb/cm^2 at 20 keV. (B) Si implanted with a nominal $1x10^{10}$ Pb/cm^2 at 20 keV. The right side of the arrow in each case is the surface position for Pb. TRIM calculations predict a Pb peak at 17.5 nm. The Cu contamination was sputtered unintentionally onto the samples from implanter beam defining slits and was also found on the starting wafers at a low level.

Fig. 4. Three TOF-HIBS spectra obtained with 150 keV N^+. Normalized yield is plotted versus flight time (decreasing from left to right). Each sample is Si dosed with Ni to nominal levels of (A) $1x10^{13}$ atoms/cm^2, (B) $2x10^{12}$ atoms/cm^2, and (C) $5x10^{11}$ atoms/cm^2. The measured amount of Ni for each is shown, as well as Br and Sb contamination peaks.

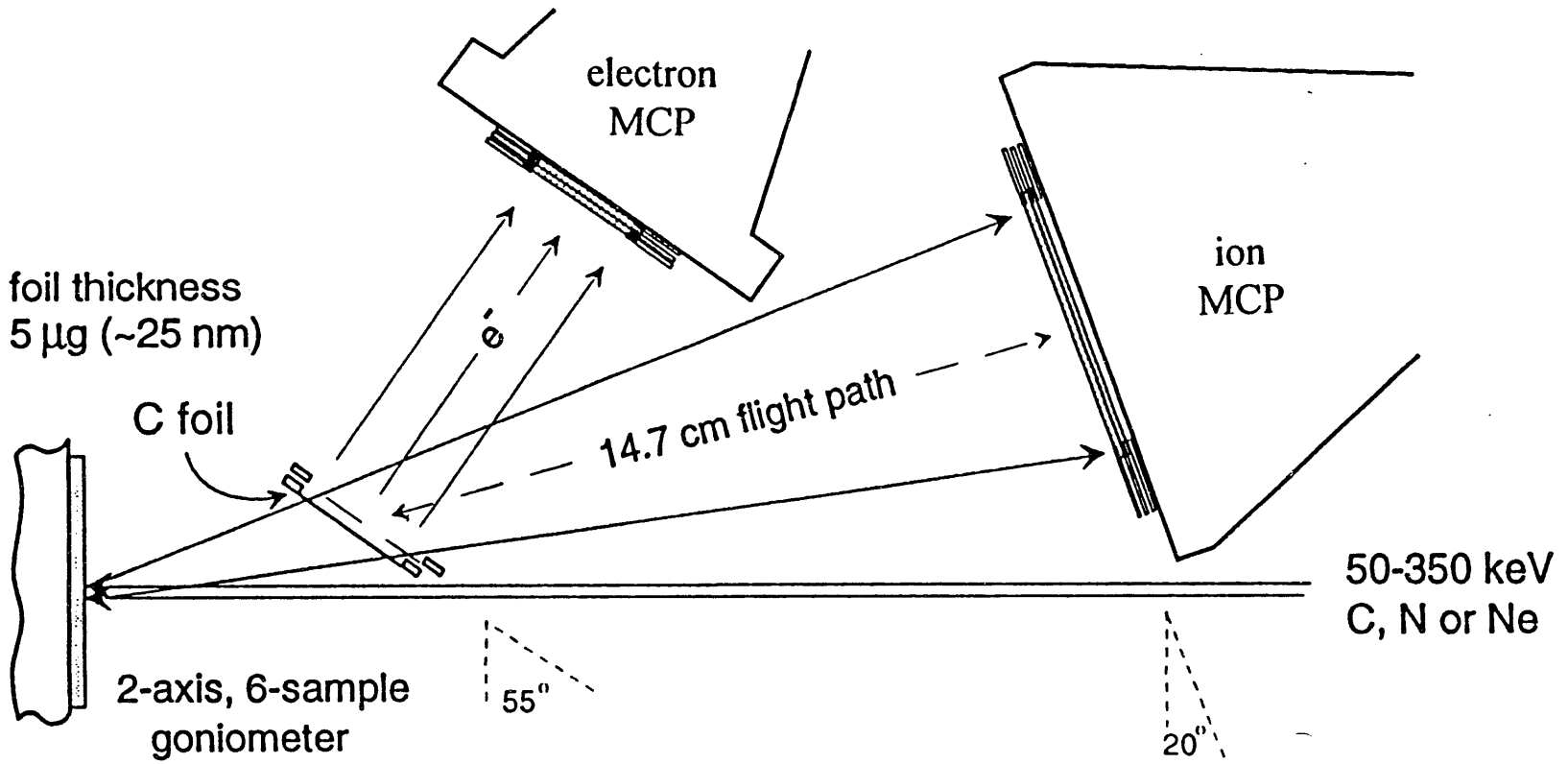
electron
MCP
ion
MCP
foil thickness
5 µg (~25 nm)
C foil
e
14.7 cm flight path
50-350 keV
C, N or Ne
2-axis, 6-sample
goniometer
55°
20°

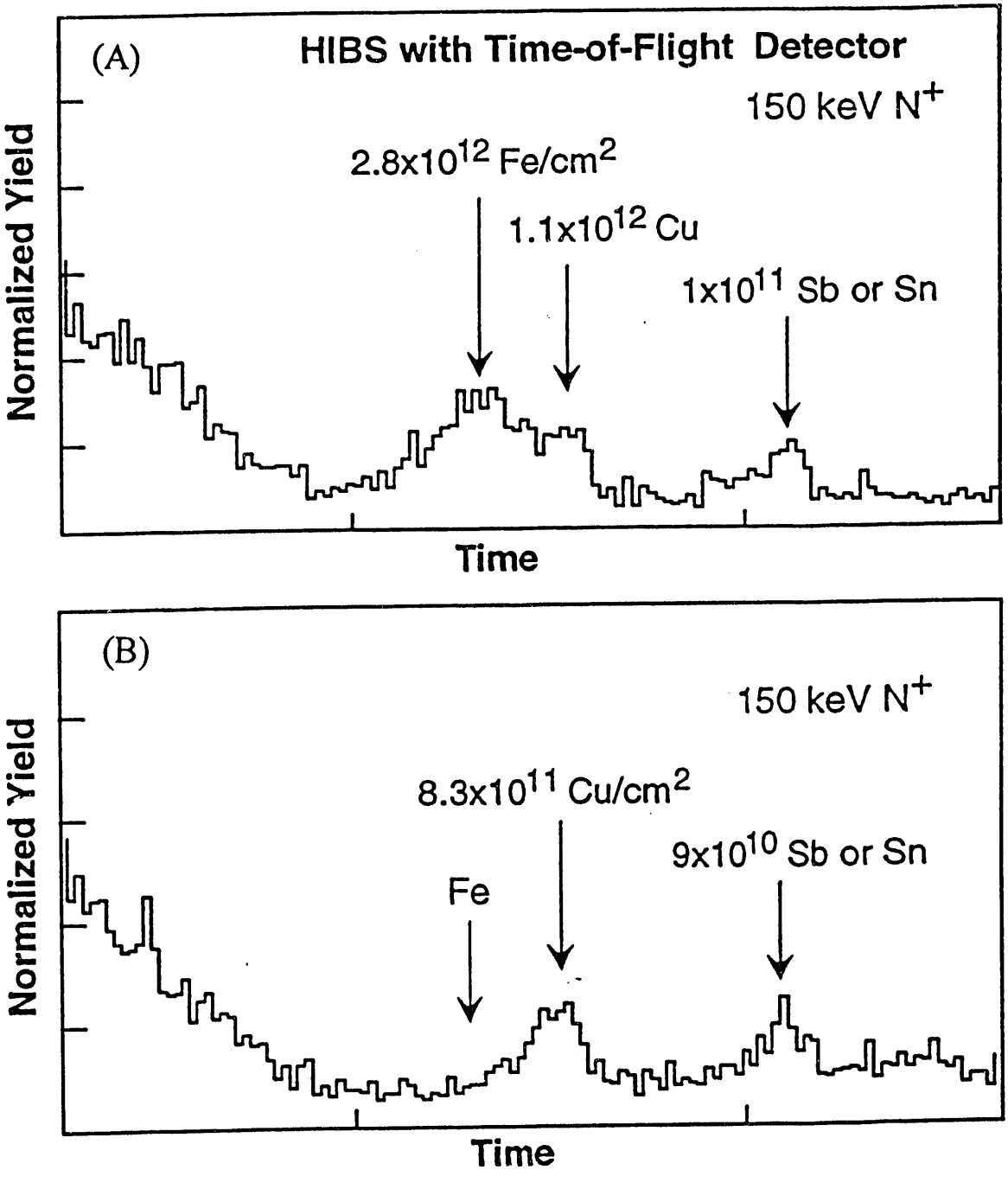
(A)
HIBS with Time-of-Flight Detector
150 keV N+
2.8x10^12 Fe/cm^2
1.1x10^12 Cu
1x10^11 Sb or Sn
Normalized Yield
Time
(B)
150 keV N+
8.3x10^11 Cu/cm^2
9x10^10 Sb or Sn
Fe
Normalized Yield
Time

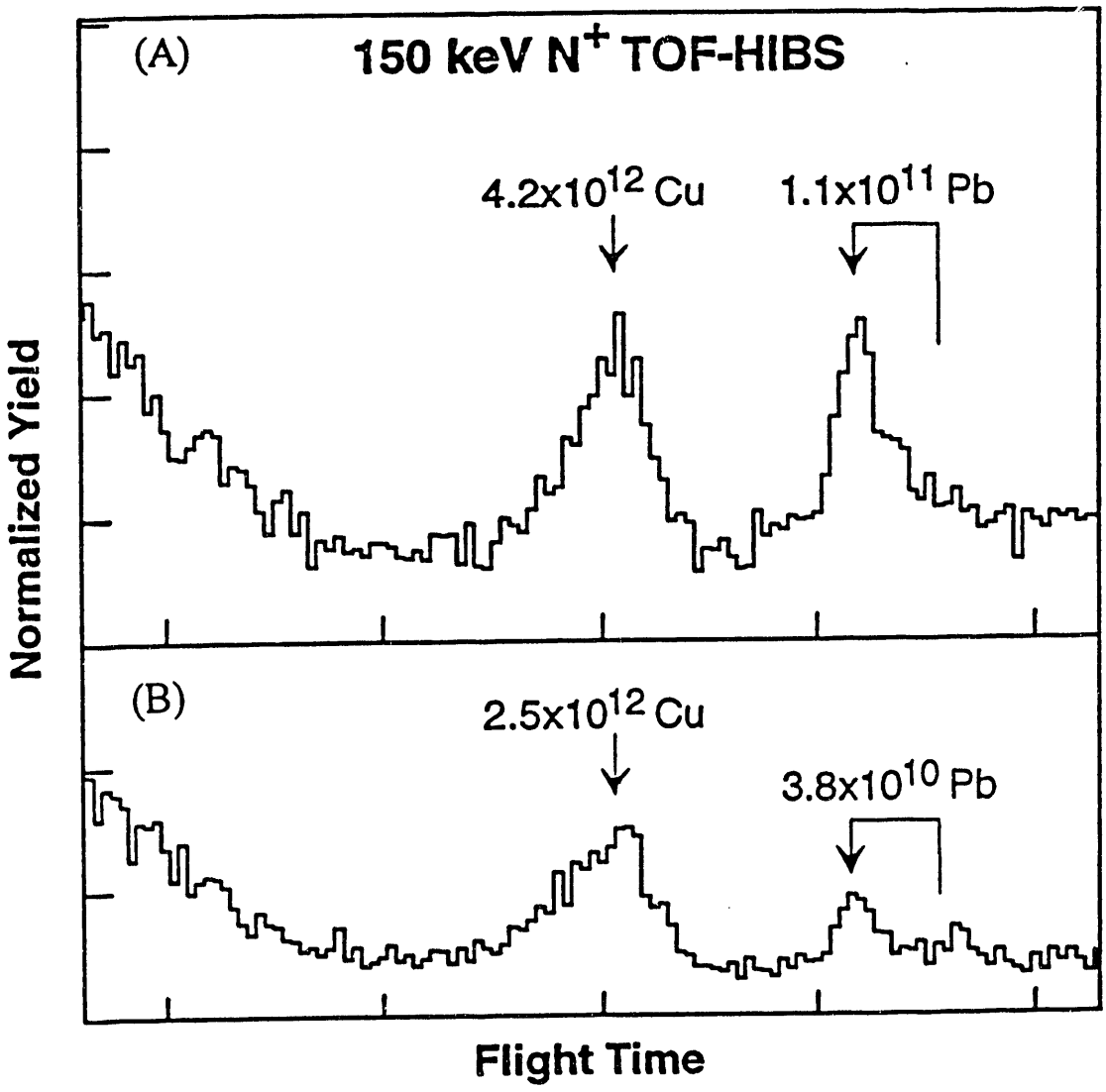
(A)
150 keV N+ TOF-HIBS
4.2x10^12 Cu
1.1x10^11 Pb
(B)
2.5x10^12 Cu
3.8x10^10 Pb
Normalized Yield
Flight Time

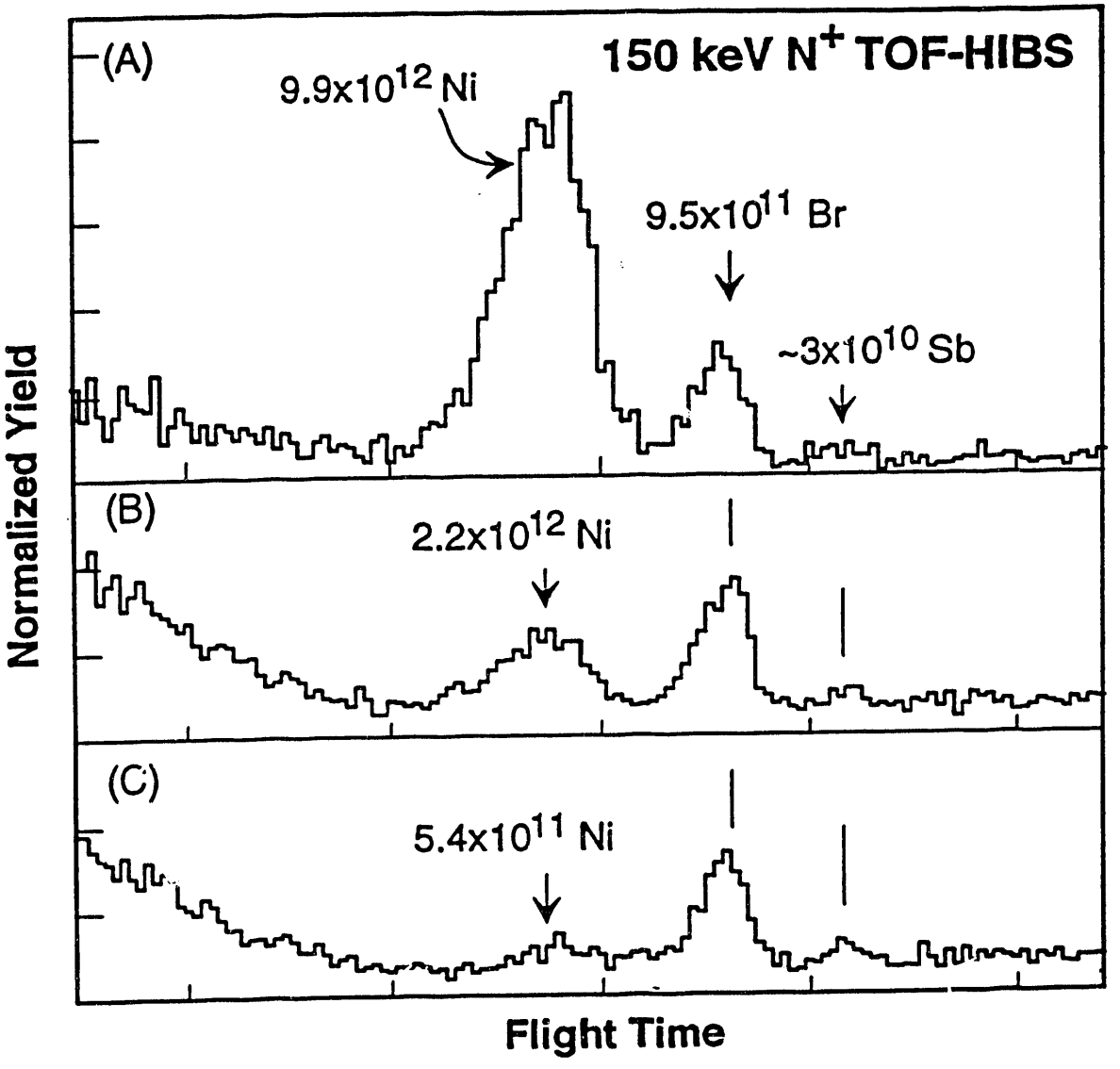
(A)
150 keV N+ TOF-HIBS
9.9x10^12 Ni
9.5x10^11 Br
~3x10^10 Sb
(B)
2.2x10^12 Ni
(C)
5.4x10^11 Ni
Normalized Yield
Flight Time

DATE
FILMED
10/20/93
END